Nanoscale Res Lett (2009) 4:627–634
DOI 10.1007/s11671-009-9290-1

NANO EXPRESS

Sol–Gel and Thermally Evaporated Nanostructured Thin ZnO Films for Photocatalytic Degradation of Trichlorophenol

A. Abdel Aal · Sawsan A. Mahmoud · Ahmed K. Aboul-Gheit

Received: 31 January 2009 / Accepted: 5 March 2009 / Published online: 19 March 2009

Abstract In the present work, thermal evaporation and sol–gel coating techniques were applied to fabricate nanostructured thin ZnO films. The phase structure and surface morphology of the obtained films were investigated by X-ray diffractometer (XRD) and scanning electron microscope (SEM), respectively. The topography and 2D profile of the thin ZnO films prepared by both techniques were studied by optical profiler. The results revealed that the thermally evaporated thin film has a comparatively smoother surface of hexagonal wurtzite structure with grain size 12 nm and 51 m^2/g. On the other hand, sol–gel films exhibited rough surface with a strong preferred orientation of 25 nm grain size and 27 m^2/g surface area. Following deposition process, the obtained films were applied for the photodegradation of 2,4,6-trichlorophenol (TCP) in water in presence of UV irradiation. The concentrations of TCP and its intermediates produced in the solution during the photodegradation were determined by high performance liquid chromatography (HPLC) at defined irradiation times. Complete decay of TCP and its intermediates was observed after 60 min when the thermal evaporated photocatalyst was applied. However, by operating sol–gel catalyst, the concentration of intermediates initially increased and then remained constant with irradiation time. Although the degradation of TCP followed first-order kinetic for both catalysts, higher photocatalytic activity was exhibited by the thermally evaporated ZnO thin film in comparison with sol–gel one.

Keywords Nanocoating · Thin films · Sol–gel · Thermal evaporation · Trichlorophenol · Water purification

A. Abdel Aal (✉)
Ecole Nationale Supérieure de Chimie de Paris,
Lab de Physico-Chimie de Surfaces, UMR-CNRS 7045, 11,
rue Pierre et Marie Curie, 75005 Paris, France
e-mail: alsayed-ibrahim@enscp.fr; foralsayed@gmail.com

A. Abdel Aal
Surface Protection & Corrosion Control Lab, Central
Metallurgical Research & Development Institute (CMRDI),
P.O. Box 87, Hellwan, Cairo, Egypt

S. A. Mahmoud · A. K. Aboul-Gheit
Process Development Division, Egyptian Research Institute,
Nasr City, PO Box 9540, Cairo 11787, Egypt

Introduction

In last decades, the presence of harmful organic compounds in water supplies and in the discharge of wastewater from chemical industries, power plants, landfills, and agricultural sources is a topic of global concern. Because of their high toxicity and their persistence, phenols and chlorinated phenols specially pentachlorophenol and trichlorophenols (2,4,5-TCP and 2,4,6-TCP) are widespread pollutants of industrial wastewaters and natural waters [1–4]. Thus, the removal of these pollutants is necessary as they contain micro impurities of polychlorinated dibenzodioxines dibenzofurans which are the most toxic of xenobiotics. Besides, chlorophenols can be transformed into more toxic compounds under the action of natural factors [5–7].

In recent years, unique chemistry of semiconductor photocatalysts is being extensively used for a variety of applications. Heterogeneous photocatalysis performed with irradiated semiconductor dispersions is one of the more interesting advanced oxidation process treatments and it is able, in most cases, to completely mineralize the organic harmful species [8]. Hence, one of the major advantages of photocatalytic process over the existing technologies is that

there is no further requirement for secondary disposal methods. The overall process can be summarized by the following reaction: Organic pollutants + O_2 → CO_2 + H_2O + mineral acid.

The advanced oxidation process depends on the production of highly reactive hydroxyl radicals ($OH^{\bullet}$) which can actively oxidize organic pollutants to minerals. Photocatalytic degradation as one of the advanced oxidation processes is based on the application of ultraviolet light in the presence of a photocatalyst. Such processes are being increasingly utilized because of simplicity, low cost, ease of controlling parameters and their high efficiency in degrading recalcitrant organic and inorganic substances in aqueous systems [9].

ZnO, as a wide-band gap semiconductor, has recently become a new research focus in the field of photoconversion applications due to its high surface reactivity [10]. ZnO can be used in different forms, like single crystals, sintered pellets and thin films. However, thin films have exhibited a wide variety of applications in environmental engineering, catalysis and gas sensor systems because they can be fabricated in small dimensions, at large scale and low cost and are widely compatible with microelectronics technology [11]. Thus, thin film photocatalysts with their high photocatalytic ability, high stability, convenient reuse, have received more and more attention [12–14].

ZnO thin films have been grown by different methods including chemical vapor deposition (CVD), magnetron sputtering, spray pyrolysis, pulsed laser deposition, chemical beam deposition, and evaporation [15–21]. However, the evaporating method is perhaps the cleanest of the entire nanoceramic synthesis route in a well-controlled atmosphere within a work chamber. On the other hand, the need to evaporate in a low-pressure environment translated directly to work chamber. Thermal evaporation is relatively simple and a low-cost technique that can be applied to low melting point, low decomposition, or low sublimation point oxides [22]. However, this technique has received very little attention from research groups.

The sol–gel process, as a simple and easy dip-coating means, is one of the versatile methods to prepare thin film-supported nano-sized particles without complicated instruments [23]. It has been well-demonstrated that the sol–gel method has considerable advantages of uniform mixing of the starting materials and good chemical homogeneity of the product. Therefore, sol–gel methods are very convenient for the preparation of thin films of high surface area amorphous oxide materials [24].

Among the semiconductors, ZnO is distinguished by its absorption over a larger fraction of the UV spectrum and the corresponding threshold of ZnO is 425 nm. Therefore, ZnO photocatalyst is considered the most suitable for photocatalytic degradation in the presence of sunlight [25]. Thus, in the present work, we have paid much attention in preparing thin films of ZnO on glass plates by a sol–gel process and thermal evaporation technique. The photocatalytic activities of the prepared catalysts were examined for the degradation of 2,4,6-TCP. The formed intermediates were determined and the degradation mechanism was discussed.

Experimental Work

ZnO Thin Films by Thermal Evaporation

Thin films of Zn were thermally grown onto glass substrates of 15 cm^2 area and 1 mm thickness under vacuum of 10^{-5} Torr, using multipurpose vacuum station (sputtering unit) VUP-5M. The growth rate and thickness were measured during growth using a crystal oscillator thickness monitor. The growth rate was adjusted to be as low as 10 nm s^{-1} to avoid differential evaporation of the metal. Thermal oxidation of Zn films using Naber therm Furnace was carried out at 550 °C for 2 h, in order to grow thin zinc oxide films on the glass substrate. Zn metal with high purity (99.9%) was used as a target and microscopic glass slide was used as a substrate.

ZnO Thin Film by Sol–Gel Method

Zinc acetate was dissolved in 2-propanol under vigorous stirring at 50–60 °C. Similarly sodium hydroxide was dissolved in 2-propanol at the same temperature under constant stirring. The zinc acetate–isopropanol solution was kept at 0 °C, then NaOH solution was added quickly under continuous stirring. The zinc oxide colloid was quite stable and no precipitate was observed. To prepare the film from this colloidal ZnO sol, glass plates of 15 cm^2 area and 1 mm thickness 15 cm^2 area and 1 mm thickness were dipped in the colloid slowly then taken out with the same speed and dried in air. The dipping process was repeated for 6 times. The dried films were finally calcined at 550 °C for 2 h.

Characterization of the Prepared ZnO Thin Film

The phase structure of ZnO films were identified by a Brucker D8-advance X-ray diffractometer with Cu K_α radiation ($\lambda = 1.5418$ Å). The surface morphology and chemical composition of ZnO films were studied using a scanning electron microscopy (JEOL-JSM-5410) equipped with energy depressive X-ray (EDX-Oxford). The topography and 2D profile of the thin ZnO films prepared by

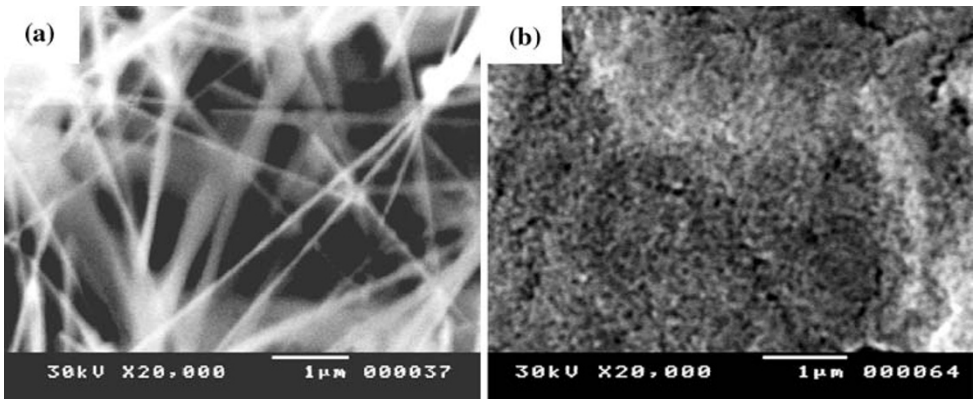

Fig. 1 SEM micrographs of ZnO thin films prepared by **a** Thermal evaporation and **b** sol–gel

both techniques were investigated by Wyko® NT Series optical profiler (Veeco Instruments, Inc.). Surface areas were recorded using Nova 2000 series based on the well-known Brunauer, Emmett and Teller (B.E.T.) theory.

Photocatalytic Degradation of TCP

An aliquot of 500 cc of an aqueous solution containing 100 ppm of high purity 2,4,6-TCP was subjected to UV irradiation using a 6 W lamp at a wavelength of 254 nm. All photodegradation experiments were conducted in a batch reactor. The UV lamp was placed in a cooling silica jacket and placed in a jar containing the polluted water. The catalyst sheet was supported in the solution with a glass holder at a controlled reaction temperature of 25 °C during the experimental period. Because photo-corrosion of ZnO frequently occurs with the illumination of UV light and this phenomenon is considered one of the main reasons for the decrease in ZnO photocatalytic activity in aqueous solutions. Thus, the photocatalytic experiments were carried out at pH 6 to ensure the highest inherent stability of catalyst [26]. At different

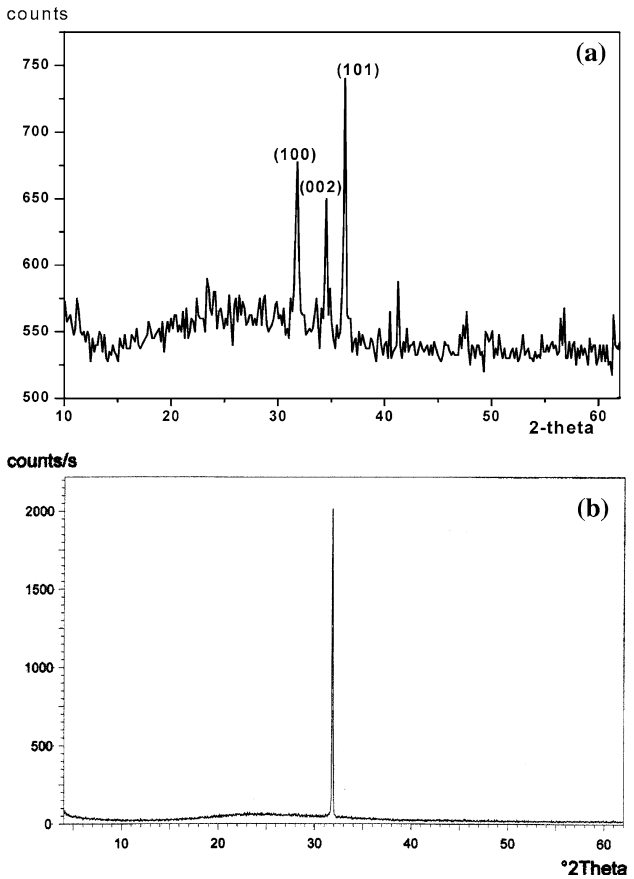

Fig. 2 XRD analysis of ZnO thin films prepared by **a** thermal evaporation and **b** sol–gel

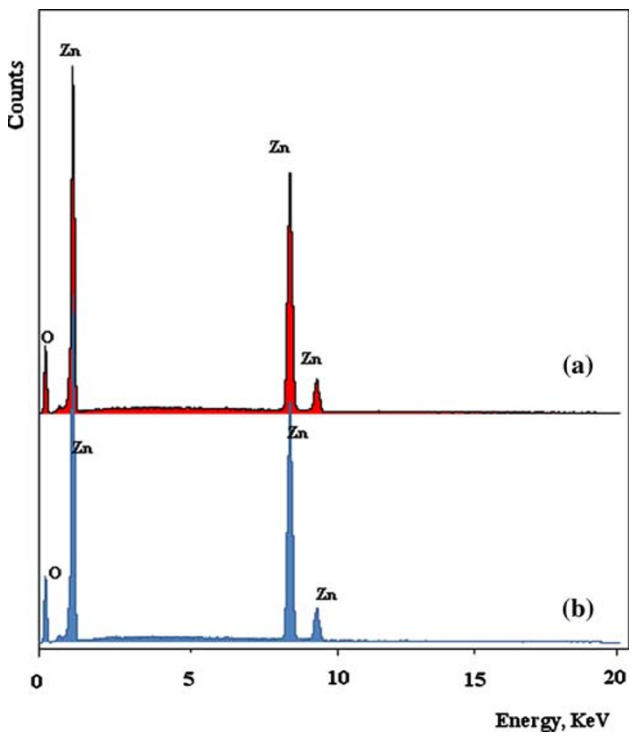

Fig. 3 EDX analysis of ZnO thin films prepared by **a** thermal evaporation and **b** sol–gel

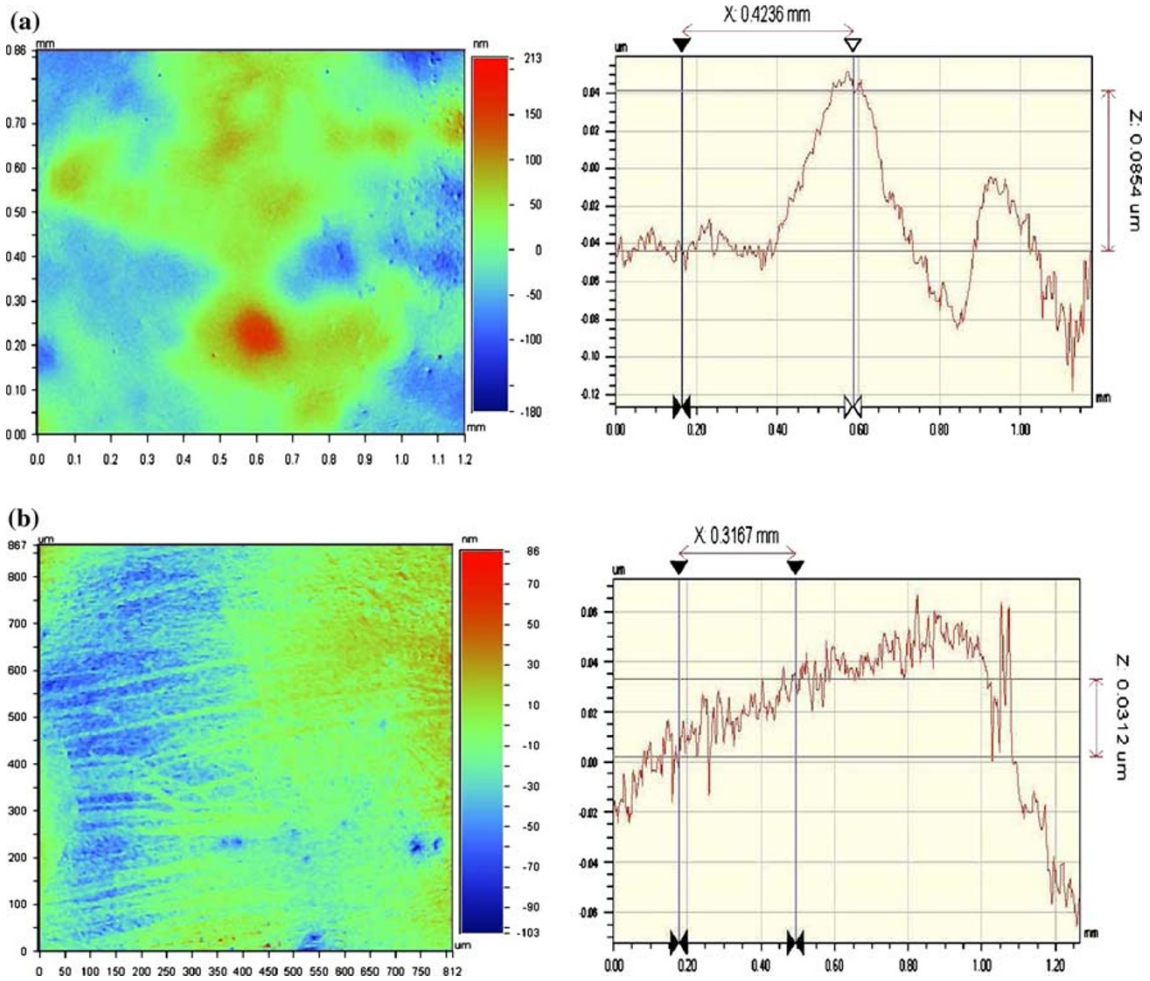

Fig. 4 Surface profile scans of ZnO thin films prepared by **a** thermal evaporation and **b** sol–gel

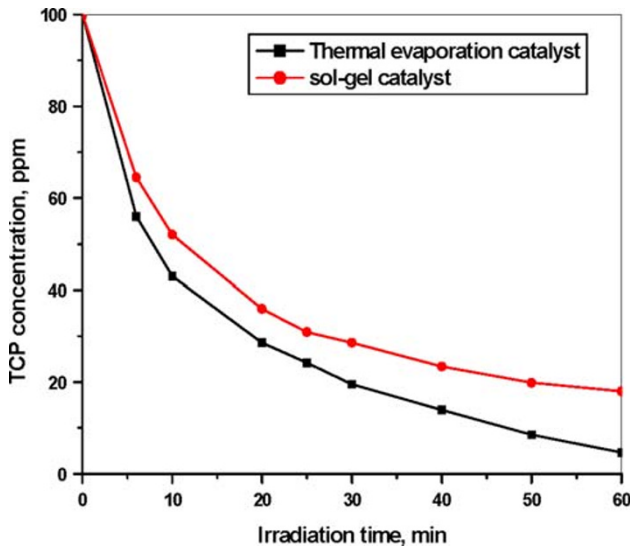

Fig. 5 Photocatalytic degradation of TCP using ZnO thin film catalyst prepared by thermal evaporation and sol–gel techniques

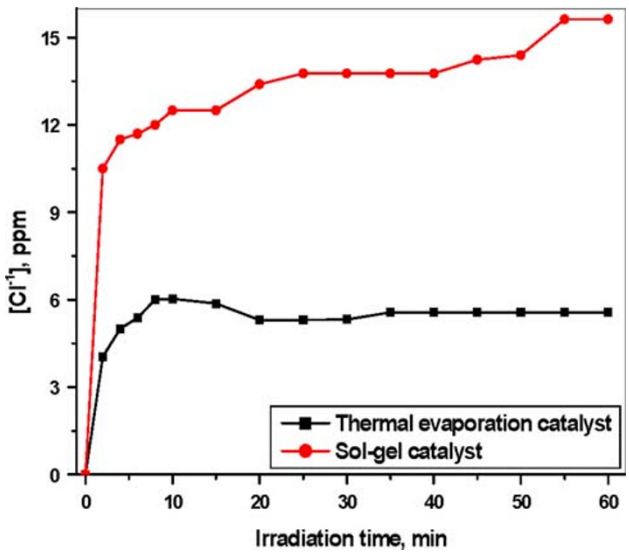

Fig. 6 Variation of $[Cl^{-1}]$ in polluted water with the irradiation time

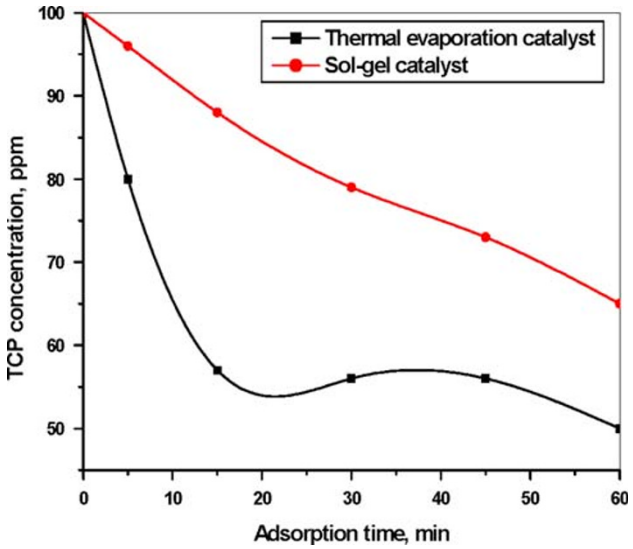

Fig. 7 Dark adsorption of TCP on ZnO thin film catalyst prepared by thermal evaporation and sol–gel techniques

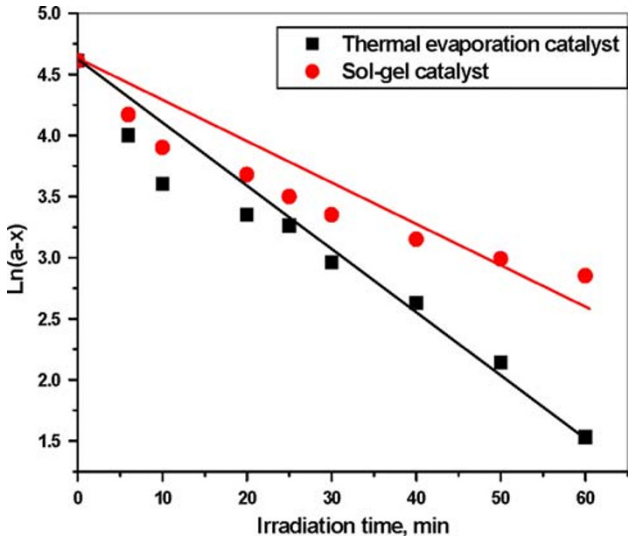

Fig. 8 Kinetics of TCP photocatalytic degradation using ZnO thin film catalyst prepared by thermal evaporation and sol–gel techniques

irradiation time intervals, samples of the irradiated water were withdrawn for analysis using an HPLC chromatograph with photo-diode-array UV detector and a C18 column. The mobile phase was acetonitrile/water (60:40) injected in a rate of 1.0 mL min^{-1}. Dionex 202 TP^{TM} C18 column (4.6 × 250) with eluent consisted of a 60:40 acetonitrile: water mixture and the flow rate was 1 mL min^{-1}. Ione chromatography (Dionex-pac) and UV detector were applied to determine the concentration of intermediates and chloride ions produced in the solution during the photodegradation.

Results and Discussion

The Characterization of ZnO Films

Thin films of Zn metal were thermally grown onto glass sheets and calcined in air at 550 °C for 2 h. On the other hand, ZnO thin film was deposited on glass sheet with same area by sol–gel and calcined under same conditions. The scanning electron micrographs of both films depicting the topography are shown in Fig. 1. For the thermally deposited films (Fig. 1a), it can be seen that the oxide consists of very thin and light long nano-fibers exhibiting all possible orientations, together with extremely small grains. In contrast to the evaporated films, the sol–gel films revealed the presence of nanometer size clusters (Fig. 1b). The film surface is well-covered without any pinholes and cracks. Such surface morphology with nanosized grains may offer increased surface area. Below, the measurement of crystallite size can be described.

The structural properties of ZnO thin films deposited by both techniques were studied by XRD and EDX analysis (Figs. 2, 3). The X-ray diffraction patterns of thin films deposited by sol–gel shows only 002 peak indicating the strong preferred orientation; the *c*-axis of the grains are uniformly perpendicular to the substrate surface. The surface energy density of the 002 orientation is the lowest in a ZnO crystal [27]. Grains with lower surface energy will become larger as the film grows. Then, the growth orientation develops into one crystallographic direction of the lowest surface energy. This means that 002 texture of the film may easily form. On the other hand, for the films deposited by thermal evaporation, three strongest XRD peaks for ZnO were detected with Miller indices (100), (002), and (101) corresponding to Bragg angles 31.8, 34.5, and 36.4°, respectively. The diffraction peaks were indexed to the hexagonal wurtzite structure (space group $P6_3mc$) and the *d*-values calculated are in good agreement with JCPDS no. 75-1526. Besides, EDX analysis confirmed the high purity of both films (Fig. 3).

The crystallite size (*t*) was estimated for both the types of films by Scherrer formula using the full-width at half maximum of the peaks corresponding to the planes (110), (002), and (101):

$$t = \frac{0.9\lambda}{B\cos(\theta_B)} \quad (1)$$

where λ is Cu (K_α) wave length, *B* is the broadening of the full-width at half maximum (F.W.H.M) and $\theta_B$is the Bragg's angle. The crystallite size for the film obtained by thermal evaporated was estimated to be about 12 nm, while the crystallite size grown by sol–gel in the *c*-axis direction was in the range of 25 nm. Thus, the thermally evaporated film has larger surface area (51 m^2/g) as compared to those

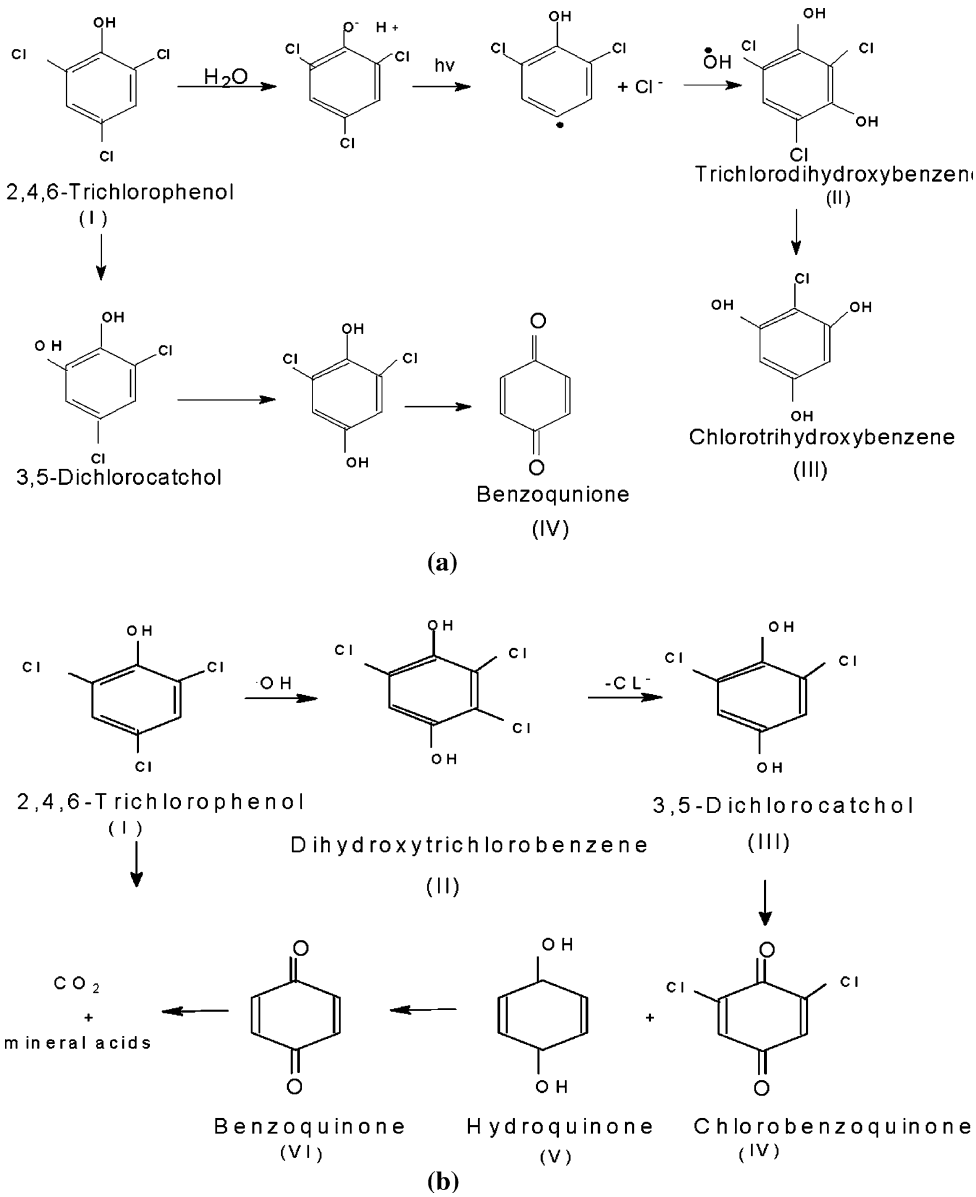

Fig. 9 Scheme for the photocatalytic degradation of TCP using ZnO thin film prepared by **a** thermal evaporation and **b** sol–gel techniques

prepared using sol–gel (27 m^2/g), which in turn affects the catalytic activity. Figure 4 illustrates the topographical image and 2D profile of the thin ZnO films prepared by both techniques. From the scans, it is clear that the thermal evaporated film has a comparatively smoother surface. The root mean square surface roughness was found to be 10 nm for the thermal evaporated films, while the roughness of sol–gel film was 30 nm.

TCP Degradation

ZnO thin films deposited by both techniques were applied for the photodegradation of 2,4,6-TCP in water. Figure 5 represents the decay of TCP with the irradiation time. Using the thermally deposited catalyst, TCP considerably degrades with time and the concentration is reduced to 4.6 ppm within 60 min from the initial concentration 100 ppm, whereas using the sol–gel catalyst, TCP decayed to 19.3 ppm. This indicates that the thermally deposited thin film photocatalyst is more efficient in TCP removal than the sol–gel one. This catalytic activity difference can be explained not only on basis of grain size measurements but also on the basis of the obtained results in terms of the chloride evolution as a function of irradiation time for both catalysts (Fig. 6). Evidently, chloride evolution, resulting from TCP degradation, is greater in case of sol–gel catalyst (14 ppm) than in the thermally deposited one (4 ppm). This higher chloride concentration probably inhibits further reactions of the adsorbed TCP molecules on sol–gel films causing the catalyst poisoning and decrease the catalytic

efficiency. In the same time, the dark adsorption of TCP on the ZnO films prepared by both thermal and sol–gel methods were studied (Fig. 7). Larger dark adsorption was observed for TCP on the thermally deposited ZnO films than sol–gel, explaining the higher rate of TCP degradation on the former catalyst. The degree of adsorption seems to correlate to the observed photodegradation rates. Figure 8 illustrates a plot of ln (a–x) against irradiation time of TCP. It can be seen that the concentration in log scale changes linearly with time indicating that the photodegradation of TCP follows the first-order kinetics. The rate constants (k_{TCP}) calculated from the slopes of the kinetic plot for the degradation reaction on thermally deposited and sol–gel catalysts are 0.0455 and 0.0272 min^{-1}, respectively. It can be concluded that the rapid degradation on the thermally deposited catalyst is likely due three reasons including: (a) the higher adsorption of TCP on the film surface which facilitates the degradation, (b) the lower chloride evolution and hence no poisoning of catalyst, (c) lower grain size and larger surface area of thermally evaporated films which improves the catalytic activity.

To investigate the degradation mechanism, the intermediate products during TCP degradation on both catalysts were determined by HPLC. The obtained analyzed data allowed the qualitative and quantitative identification of these intermediates is demonstrated in scheme a, b in Fig. 9. Therefore, Fig. 10 shows the variation of intermediates concentration formed during TCP degradation on sol–gel ZnO films. It is obvious that the concentration of a major compound increases with irradiation time reaching 18.0 ppm at 40 min and then remains constant with a further increase of irradiation time. This intermediate is formed from TCP via dechlorination to trichlorodihydroxybenzene (compound II in scheme a). A second intermediate covering most of the irradiation run (10–60 min) with a concentration of almost 5.0 ppm. As indicated by HPLC, this compound is most probably chlorocatechol. A third intermediate appeared with a concentration increasing linearly from the beginning as a function of irradiation time. On the sol–gel catalyst, hydroquinone and benzoquinone do not appear as a photointermediate products using ZnO prepared via thermal evaporation technique (Fig. 11). However, none of the three intermediates identified exhibited a tendency of declining with increasing the irradiation time, which may explain the lower activity of this sol–gel prepared catalyst.

Notably, during the photodegradation of TCP, most of the intermediates corresponds to the substitution in the Para or Ortho positions of the phenol ring while higher concentration of the intermediates was observed of Para substituted position in case of the sol–gel. This indicates to the preferable attach of Para position. The $^{\bullet}OH$ substitution removes chloride bond of the ring leads to the formation of benzoquinone (BQ) and hydroquinone in the case of thermal evaporation [28]. Dihydroxychlorobenzene as a major intermediate using sol–gel catalyst is formed due to its high activity in the dechlorination (C–Cl cleavage). This intermediate is not formed using thermal evaporation due to its high activity in the destruction of the benzene ring rather than C–Cl bond i.e., different methods of preparation leads to different pathway for the degradation.

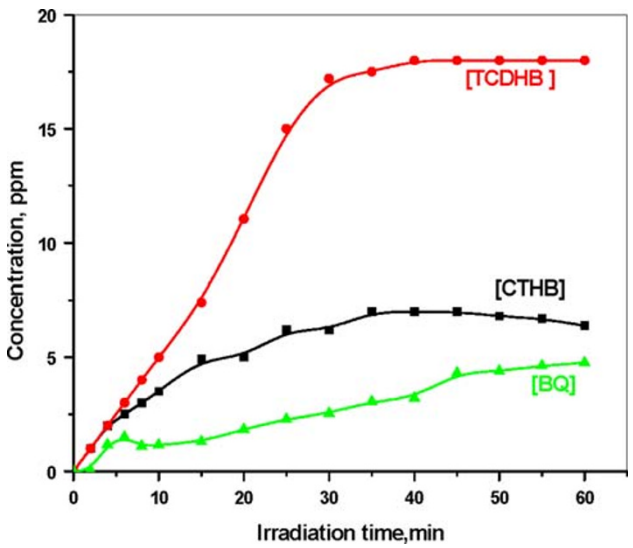

Fig. 10 Formation of trichlorodihydroxybenzene (TCDHB), chlorotrihydroxybenzene (CTHB), and benzoquinone (BQ) during the photocatalytic degradation of TCP using ZnO thin film prepared via sol–gel technique

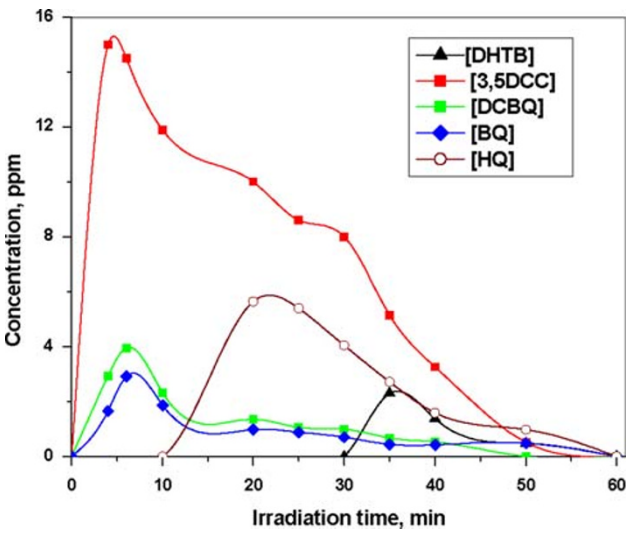

Fig. 11 Formation of dihydroxytrichlorobenzene (DHTB), 3,5 dichlorocatecol (3,5DCC), dichlorobenzoquinone (DCBQ), benzoquinone (BQ), and hydroquinone (HQ) during TCP photodegradation using thermal evaporated ZnO catalyst

Conclusions

- Thermal evaporation and sol–gel techniques were applied for the fabrication of nanostructured ZnO thin films.
- Thermal evaporated films have less surface roughness and lower grain size in comparison with sol–gel films calcined at same conditions.
- XRD analysis for both catalysts indicated to the strong preferred orientation of sol–gel ZnO thin films and the hexagonal wurtzite structure of thermal evaporated films.
- The degradation of TCP followed first-order kinetics for both catalysts. However, the thermally deposited thin film photocatalyst is more efficient in TCP removal than the sol–gel one because of less grain size (or higher surface area) and less chloride evolution which causes the catalyst poisoning.

References

1. I. Ochuma, R. Fishwick, J. Wood, J. Winterbottom, J. Hazard. Mater. **144**, 627 (2007). doi:10.1016/j.jhazmat.2007.01.086
2. S. Chaliha, K. Bhattacharyya, Chem. Eng. J. **139**, 575 (2008). doi:10.1016/j.cej.2007.09.006
3. Y. Nie, C. Hu, J. Qu, X. Hu, J. Hazard. Mater. **154**, 146 (2008). doi:10.1016/j.jhazmat.2007.10.005
4. M. Li, P. Tang, Z. Hong, M. Wang, Colloid Surf. Physicochem. Eng. Aspect **318**, 285 (2008). doi:10.1016/j.colsurfa.2008.01.001
5. Y. Skurlatov, L. Ernestova, E. Vichutinskaya, D. Samsonov, I. Semenova, I. Rodko, V.O. Shvidky, R.I. Pervunina, T. Kemp, J. Photochem. Photobiol. A Chem. **107**, 207 (1997). doi:10.1016/S1010-6030(97)00011-7
6. A. Svenso, L. Kjeller, C. Rappe, Environ. Sci. Technol. **23**, 900 (1989). doi:10.1021/es00065a022
7. C. Park, C. Menini, J. Valverde, M. Keane, J. Catal. **211**, 451 (2002). doi:10.1006/jcat.2002.3750
8. T. Pandiyan, O. Martinez Rivas, J. Martinez, G. Amezcua, M. Martinez-Carrillo, J. Photochem. Photobiol. A Chem. **146**, 149 (2002). doi:10.1016/S1010-6030(01)00606-2
9. A. Eslami, S. Nasseri, B. Yadollahi, A. Mesdaghinia, F. Vaezi, R. Nabizadeh, S. Nazmara, J. Chem. Technol. Biotechnol. **83**, 1447 (2008). doi:10.1002/jctb.1919
10. A. Djurisic, Mater. Sci. Eng. B **38**, 237 (2002). doi:10.1016/S0927-796X(02)00063-3
11. M. Suchea, S. Christoulakis, M. Katharakis, G. Kiriakidis, N. Katsarakis, E. Koudoumas, Appl. Surf. Sci. **253**, 8141 (2007). doi:10.1016/j.apsusc.2007.02.163
12. A. Abdel Aal, M. Barakat, R. Mohamed, Appl. Surf. Sci. **254**, 4577 (2008). doi:10.1016/j.apsusc.2008.01.049
13. J. Byrne, B. Eggins, M. Brown, B. McKinney, M. Rous, Appl. Catal. B **17**, 25 (1998). doi:10.1016/S0926-3373(97)00101-X
14. J. Herrmann, H. Tahiri, Y. Ait-Ichou, G. Lassaletta, A. Gonzalez-Elipe, A. Fernandez, Appl. Catal. B **13**, 219 (1997). doi:10.1016/S0926-3373(96)00107-5
15. B. Juárez, P. García, D. Golmayo, A. Blanco, C. López, Adv. Mater. **17**, 2761 (2005). doi:10.1002/adma.200500569
16. C. Lizama, J. Freer, J. Baeza, H. Mansilla, Catal. Today **76**, 235 (2002). doi:10.1016/S0920-5861(02)00222-5
17. J. Chang, H. Wang, M. Hon, J. Cryst. Growth **211**, 93 (2000). doi:10.1016/S0022-0248(99)00779-4
18. K. Reddy, H. Gopalaswamy, P. Reddy, R.W. Miles, J. Cryst. Growth **210**, 516 (2000). doi:10.1016/S0022-0248(99)00868-4
19. H. Kim, C. Gilmore, J. Horwitz, A. Piqué, H. Murata, G. Kushto, R. Schlaf, Z. Kafafi, D. Chrisey, Appl. Phys. Lett. **76**, 259 (2000). doi:10.1063/1.125740
20. M. Wang, L. Zhang, Mater. Lett. **63**, 301 (2009). doi:10.1016/j.matlet.2008.10.022
21. M. Jin, J. Feng, Z. Heng, M. Li, L. Ying, Thin Solid Films **357**, 98 (1999). doi:10.1016/S0040-6090(99)00357-0
22. S. Panda, N. Singh, J. Hooda, C. Jacob, Cryst. Res. Technol. **43**, 751 (2008). doi:10.1002/crat.200711126
23. P. Siciliano, Sens. Actuators B Chem. **70**, 153 (2000). doi:10.1016/S0925-4005(00)00585-2
24. C. Raj, M. Lincoln, S. Das, Cryst. Res. Technol. **43**, 823 (2008). doi:10.1002/crat.200811165
25. M. Behnajady, W. Modirshahla, N. Daneshvar, M. Rabbani, J. Hazard. Mater. **140**, 257 (2007). doi:10.1016/j.jhazmat.2006.07.054
26. R. Comparelli, E. Fanizza, M. Curri, P. Cozzoli, G. Mascolo, A. Agostiano, Appl. Catal. B Environ. **60**, 1 (2005). doi:10.1016/j.apcatb.2005.02.013
27. K. Chopra, S. Major, D. Pandaya, Thin Solid Films **102**, 1 (1983). doi:10.1016/0040-6090(83)90256-0
28. C. Turchi, D. Ollis, J. Catal. **122**, 178 (1990). doi:10.1016/0021-9517(90)90269-P